THE JOURNAL OF BIOLOGICAL CHEMISTRY
Vol. 279, No. 21, Issue of May 21, pp. 22461–22468, 2004
Printed in U.S.A.

A Novel Human Cl^- Channel Family Related to *Drosophila flightless* Locus*

Received for publication, December 17, 2003, and in revised form, March 8, 2004
Published, JBC Papers in Press, March 8, 2004, DOI 10.1074/jbc.M313813200

Makoto Suzuki‡ and Atsuko Mizuno

From the Department of Pharmacology, Jichi Medical School 3311-1, Yakushiji, Minamikawachi, Tochigi 329-0498, Japan

Large conductance chloride (maxi-Cl^-) currents have been recorded in some cells, but there is still little information on the molecular nature of the channel underlying this conductance. We report here that *tweety*, a gene located in *Drosophila flightless*, has a structure similar to those of known channels and that human homologues of *tweety* (hTTYH1–3) are novel maxi-Cl^- channels. hTTYH3 mRNA was found to be distributed in excitable tissues. The whole cell current of hTTYH3 was large enough to be discriminated from the control but emerged only after treatment with ionomycin. Analysis of pore mutants suggested that positively charged amino acids contributed to anion selectivity. Like a maxi-Cl^- channel *in situ*, the hTTYH3 single channel showed 26-picosiemen linear current voltage, complex kinetics, 4,4′-diisothiocyanato-stilbene-2,2′-disulfonic acid sensitivity, subconductance, and the permeability order of $I^- > Br^- > Cl^-$. Similarly, hTTYH2 encoded an ionomycin-induced maxi-Cl^- channel, but TTYH1 encoded a Ca^{2+}-independent and swelling-activated maxi-Cl^- channel. Therefore, the hTTYH family encoded maxi-Cl^- channels of mammals. Further studies on the hTTYH family should lead to the elucidation of physiological and pathophysiological roles of novel Cl^- channel molecules.

Chloride (Cl^-) anion passes through the cell membrane in greatest abundance mainly by channels. Cl^- channels play roles in the stabilization of membrane potential, transport, and cell volume regulation. Cl^- channels are observed in many tissues and are thus variably regulated by voltage, calcium, pH, or cell volume. There are three types of Cl^- channels based on their conductance: small (<10 pS),[1] medium (10–100 pS), and large (100 >pS, maxi-Cl^-) conductance channels. Small and medium conductance channels are found ubiquitously, even in oocytes, whereas large conductance channels are rarely found. To our knowledge, less than 12 cells possessing maxi-Cl^- channels have been found over the past 40 years. A maxi-Cl^- channel in muscle or in other tissues is activated directly by cytosolic Ca^{2+} (1, 2), whereas activity of the channel in other tissues is independent of Ca^{2+} (3, 4). GTP-binding protein (5), cell volume (3), and protein kinases (6) have been reported to modify the function of a maxi-Cl^- channel. However, because of their rarity, the physiological role of maxi-Cl^- channels remains obscure.

The molecular structures of Cl^- channels are diverse, with different transmembrane segments (TMSs) such as cystic fibrosis transmembrane regulator (7) and ClC (8) with 10 or 12 TMSs. Aquaporin-6 encodes a unique acid-dependent Cl^- channel with 6 TMSs (9). The ClCA family, with 5 TMSs, encodes medium conductance Ca^{2+}-activated Cl^- (CaC) channels (10, 11). Thus, it is possible that there exists a Cl^- channel with more variable TMSs.

On the other hand, cDNA encoding ion channels is generally expressed in ovary cells, such as Chinese hamster ovary (CHO) and *Xenopus* oocytes. They possess Cl^- channels endogenously. CaC currents are frequently observed as endogenous currents of these cells. The CaC current is driven by small or medium conductance Cl^- channels activated by a high concentration of intracellular Ca^{2+}, is outwardly rectifying, and is inhibited by 4,4′-diisothiocyanato-stilbene-2,2′-disulfonic acid (DIDS) and niflumate (3). Human embryonal kidney (HEK) cells have also been used for the expression of cDNA encoding CaC (10), but they possess endogenous maxi-Cl^- channels regardless of the concentration of Ca^{2+} (12).

To try to find a novel ion channel, we used the BLAST program to search for proteins that have four or more TMSs as predicted by hydrophobicity and a gene related to behavior abnormality. By using a cluster of leucine residues as a transmembrane probe, we found a human gene (*httyh3*) that has homology to *Drosophila tweety* (*dttyh1*) located in the *flightless* locus (13), which is related to behavior abnormality. *flightless* is a mutant of *Drosophila melanogaster*. The flightless gene is molecularly characterized by four transcription units within it, which are named tweety (*twe*), *fli*, dodo (*dod*), and penguin (*pen*). These genes are required for normal flight. We therefore investigated the localization and expressed currents of hTTYH3 in the present study.

MATERIALS AND METHODS

Isolation and Detection of hTTYH3—Human TTYH3 cDNA (AL530584) was purchased from Incyte Genomics. Mutants were made by using PCR (QuickChange, Stratagene). Northern blot analysis was performed with a membrane (human multiple tissues Northern blot, Clontech, Tokyo, Japan) according to the manufacturer's protocol using a PstI fragment as a probe. Mouse RNA was isolated by using the guanidine thiocyanate method with organic extraction (Trizol, Invitrogen). A mouse TTYH3 (mTTYH3) fragment was cloned by PCR followed

* The costs of publication of this article were defrayed in part by the payment of page charges. This article must therefore be hereby marked "*advertisement*" in accordance with 18 U.S.C. Section 1734 solely to indicate this fact.

The nucleotide sequence(s) reported in this paper has been submitted to the DDBJ/GenBank™/EBI Data Bank with accession number(s) AB162931, BC005168, AB162929, AB162930, and NM020659.

‡ To whom correspondence should be addressed: Dept. of Pharmacology, Jichi Medical School 3311-1, Yakushiji, Minamikawachi, Tochigi 329-0498, Japan. Tel.: 81-285-58-7326; Fax: 81-285-44-5541; E-mail: macsuz@jichi.ac.jp.

[1] The abbreviations used are: pS, picosiemens; CHO, Chinese hamster ovary; FITC, fluorescent isothiocyanate; SITS, 4-acetamido-4′-isothiocyanatostilbene-2,2′-disulfonic acid; DIDS, 4,4′-diisothiocyanatostilbene-2,2′-disulfonic acid; HEK, human embryonal kidney; TMSs, transmembrane segments; TEA, tetraethylammonium; GTPγS, guanosine 5′-3-*O*-(thio)triphosphate; RT, reverse transcriptase; CaC, Ca^{2+}-activated Cl^-; m, mouse; h, human; GFP, green fluorescent protein.

by reverse transcriptase (RT) using a primer set (5′-AAGCTGTCGGGCAGCCACAA-3′ and 5′-CGATGGAGCTGAACATGAGG-3′) that detects an 84-amino acid fragment from S positions 310–394. RT-PCR detections of human, hamster (*Cricetulus griseus*), and mouse TTYH3 (hmcTTYH3) exons in the cell lines and tissues were performed by conventional methods. Human endothelial cells (number 375) and smooth muscle cells (number 716) were purchased from Applied Cell Biology Research Institute. Neuronal cells (PC12 and N2A) were gifts from K. Shimazaki (Department of Neurophysiology, Jichi Medical School, Japan).

The mTTYH3 protein was detected in mouse tissues. Specific antibodies were raised against the C-terminal region of MRAKYLATSQ, which was common in human, hamster, and mouse clones. An antigen (1 mg/ml distilled water) conjugated with 1 ml of Freund's adjuvant was intramuscularly injected into New Zealand White rabbits, and this was followed by biweekly booster injections of the same dose of the antigen in Freund's incomplete adjuvant. Serum in which the titer was over 10,000 times higher than that of the control was obtained 8 weeks later. The immunized rabbit serum was passed through a column (Amersham Biosciences) and affinity-purified by a kit (Pierce) according to the manufacturer's protocol. Extracts of subconfluent HEK293 or CHO cells (in 60-mm dishes) with or without transfection of hTTYH3 cDNA were lysed by gentle sonication in 50 mM NaH_2PO_4, 300 mM NaCl, 10 mM imidazole, 0.05% Tween 20 (pH 8.0), and protease inhibitors. Digestion was performed with the proteins at a concentration of 20 mg/20 ml and incubated with *N*-glycanase (0.5 units/20 μl) for 18 h at 37 °C. Western blot analysis with a blocking test by an excess of antigen (1 μg/ml) was performed to evaluate specificity. Immune complexes were detected by horseradish peroxidase-labeled anti-rabbit IgG by using an ECL detection system (PerkinElmer Life Sciences). Histologic staining was performed by conventional methods and detected by fluorescent isothiocyanate (FITC)-labeled anti-rabbit IgG (Dako, Kyoto, Japan). The tissues were viewed through a microscope (BX-5, Olympus, Tokyo, Japan), and photographs were stored in a computer.

Expression of cDNA—A plasmid expressing green fluorescence protein (pEGFP-N1, Clontech, Tokyo, Japan) or red fluorescence protein (pDsRed1-N1, Clontech) was used as a marker for transfection. 0.5 μg of the marker cDNA and 1 μg of hTTYH3 cDNA or its mutants were transfected into mammalian cells grown on coverslips using FuGENE6™ (Roche Applied Science). Growth and transfection were performed in 10% fetal calf serum-containing media. The cells were used without any further treatment for patch clamp samples. The experiments were performed at 48–72 h after the transfection.

To make stable transformed cells, we inserted hTTYH3 cDNA into a plasmid (pIREShygr3, Clontech). The CHO cells were transfected by electroporation, and the stable transformant was cloned using the immunoreactivity as a marker.

Electrophysiology—Patch clamp recordings were carried out according to conventional methods (14). The experiments were performed at room temperature (20–25 °C). Micropipettes were made from capillary tubes (Drummond Scientific, Broomall, PA) that were coated by beeswax before fire-polishing. They had a resistance of <10 megohms. Series resistance in a whole cell configuration was around 300 megohms. The GFP-positive cells were visualized by fluorescence measurement (CAM 2000 System, Jasco, Tokyo, Japan) with an emission of 490 nm. Currents were recorded with an EPC-9 patch clamp amplifier (HEKA, Pfalz, West Germany). Applied voltage and sampling (10 kHz) were controlled by a computer system (HEKA, Pfalz, West German). Samples were filtered through 1 kHz, and analysis was performed using the software Patch Analyst Pro. The bath solution contained 140 mM NaCl (or TEA-Cl or sodium gluconate), 1.0 mM $MgCl_2$, and 3 mM HEPES (pH 7.4). The whole cell patch pipette contained a filtered solution of 140 mM CsCl, 1.0 mM $MgCl_2$, and 3 mM HEPES (pH 7.2) with or without 0.5 mM $CaCl_2$. To calculate the ratio of X^- to Cl^- permeability in a whole cell configuration, the current-clamp mode was used to measure reversal potential. Then the reversal potential was compensated by liquid junction potential, and the ratio was calculated by using an equation (15). For single channel analysis, the pipette solution was changed to 140 mM Na*X*, 1.0 mM $MgCl_2$, and 3 mM HEPES (pH 7.4). Single channel recording was performed in inside-out patches, and then reversal potential was calculated to obtain the selective permeability. To obtain the desired Ca^{2+} concentration, Ca/EGTA concentration in the solution for the cytoplasmic side was adjusted with appropriate amounts of KCl, KOH, $MgCl_2$, and HEPES, keeping a constant ionic strength (Σ ions^2) of 1.5. A hypotonic solution was made by addition of distilled water to the bath solution. Osmolality was measured using an osmometer (One-Ten Osmometer, Fiske, MA).

The data were analyzed using one-way analysis of variance, and the significance was calculated using Bonferroni's analysis. $p < 0.05$ was considered statistically significant.

RESULTS

Isolation and Characterization of hTTYH3 Protein—The sequence of the purchased cDNA (AL530584) had significant homology to *ttyh1* and *ttyh2* (NM020659 and NM032646) and was named *ttyh3*. The gene *ttyh3* is located in 7p22.3. Other family members of *ttyh3* were found by using the BLAST program; one was found in *Drosophila* (CG3638) and two were found in *Homo sapiens* (*ttyh1* and *ttyh2*). hTTYH3 mRNA encodes 4800 nucleotides and 523 amino acids. hTTYH1 is thought to have 5 TMSs (16), whereas hTTYH3 is thought to possess 6 TMSs. Both were predicted by the Sosui program (GenomNet, Kyoto University) (Fig. 1*A*). The third TMS (TMS3) was predicted in hTTYH3 but not in hTTYH1. The cluster of leucine used for the search was found in TMS4. To determine the membrane topology, a marker (His_6) was inserted between TMS3 and TMS4 (amino acids 199–209) and between TMS5 and TMS6, which were expressed in mammalian cells and then detected with an FITC-labeled antibody against His_6 (data not shown). The mutants containing the marker in the given positions (amino acids 202, 205, 208, and 257, Fig. 1*A*, *green triangles*) were positive, and the other mutants (*red triangles*) were negative for binding when the antibody was incubated outside the cells. However, addition of His_6 may change the transmembrane topology.

Detection of an *ttyh3* product and glycosylation scanning were performed with an antibody raised against C-terminal peptides. The amino acid sequence of the C-terminal region used for the antibody is a common sequence among hamsters, mice, and humans. Western blot analysis showed positive signal in expressed CHO cells (Fig. 1*B*), whereas immunoreactivity was not detected in control CHO cells. On the other hand, immunoreactivity was faintly detected by Western blotting and clearly detected by immunohistochemistry in HEK cells (Fig. 1*C*), suggesting that hTTYH3 is an endogenous Cl^- channel. Incubation of the same membrane with an excess of antigen (1 μg/ml) abolished the signals, indicating that the antibody is specific for hTTYH3 detection. Possible glycosylation sites (Asn-Xaa-Thr/Ser, *red circle*) were found at the positions 128, 144, and 353. Glycosylation scanning was performed by using *N*-glycanase digestion. The protein of hTTYH3 expressed in CHO was incubated with *N*-glycanase, resulting in digestion of the upper band, but the sequence-predicted 58-kDa band remained. Thus, the upper band in CHO was a glycosylated form of hTTYH3. When threonine was substituted by alanine at the three sites, Thr at position 353 was the only site glycosylated. Thr at 353 was therefore located in an extracellular domain. Therefore, the structure of hTTYH3 is like that illustrated in Fig. 1*A* (*lower panel*), regardless of whether TMS3 (*white column*) penetrates the membrane or not.

The putative structure of hTTYH3 may be comparable with that of the Ca^{2+}-activated large conductance potassium channel (17, 18) (maxi-K^+, Fig. 1*A*, *lower*). The pore region in maxi-K^+ determines potassium ion selectivity located between TMS5 and TMS6. The position of the pore region in hTTYH3 is predicted to be similar to that of maxi-K^+, where positively charged amino acids, arginine and histidine, are commonly conserved in the TTYH family. Maxi-K^+ has a unique aspartate cluster below the last transmembrane domain. This negatively charged cluster is called the "Ca^{2+} bowl" and is related to direct activation by Ca^{2+} (18). A Ca^{2+} bowl-like sequence was recognized in the TTYH family as a glutamate- or Asp-rich domain. Knockout of the maxi-K^+ channel gene resulted in a "slowpoke," whereas that of the *tweety* gene resulted in a "flightless" in *Drosophila*; both genes are related to behavior abnormality.

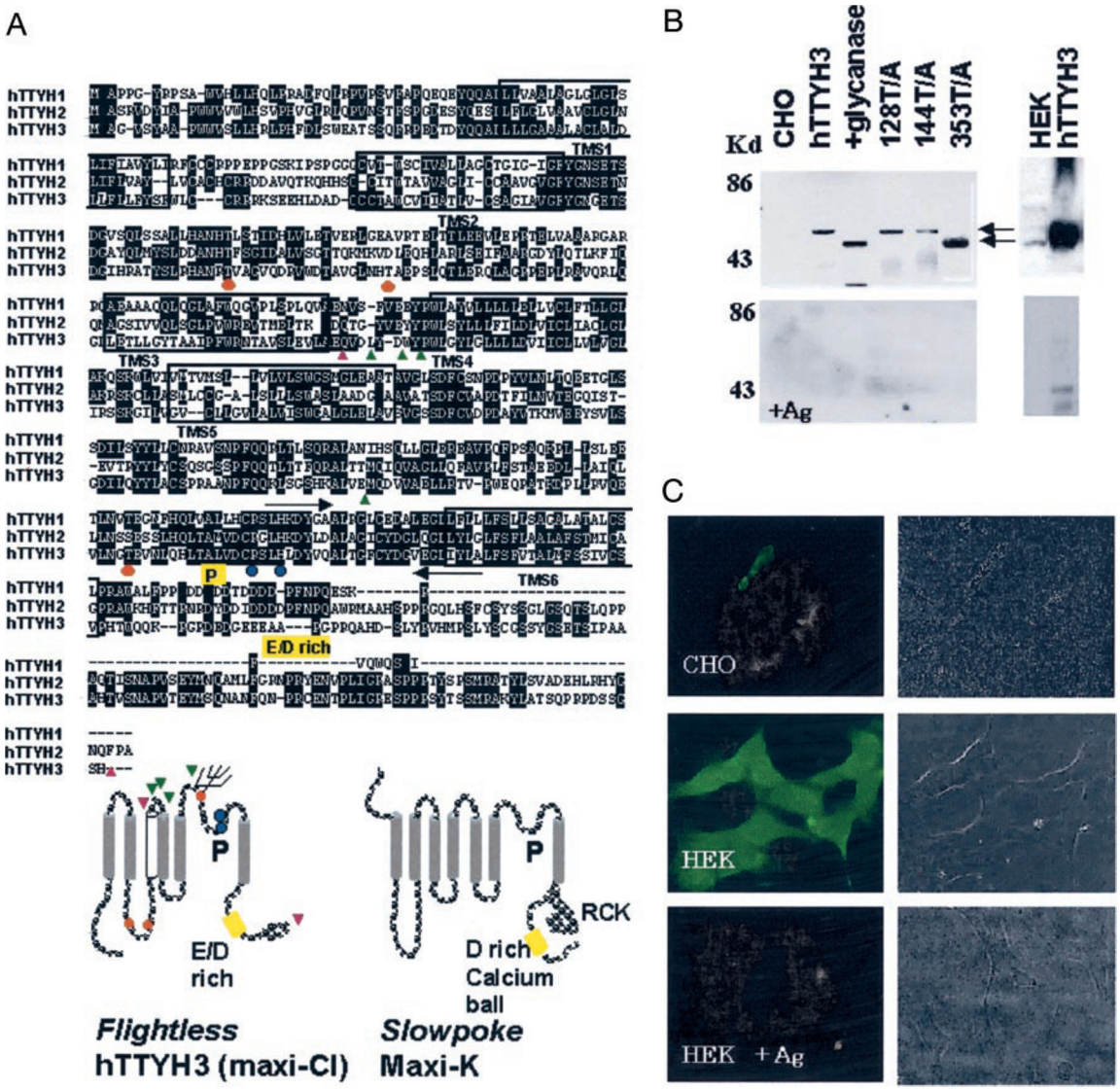

FIG. 1. **Amino acid alignment of the hTTYH family.** *A*, amino acid alignment of the human TTYH family (hTTYH1–3, hTTYH1, NM020659; hTTYH2, NM032646, hTTYH3, AL530584) is shown. Possible transmembrane segments (TMS1–6, *boxes*), marker for membrane topology (*triangle*), pore region (*P*) with negatively charged amino acids (*blue circle*), possible glycosylation sites (*red circles*), and Glu/Asp-rich C-terminal region (*yellow*) are illustrated. The primers for RT-PCR are indicated by *arrows.* The *lower schema* shows the proposed hTTYH3 structure in *Drosophila flightless* encoding a large conductance channel (maxi-Cl^-) in comparison to the structure of a large conductance Ca^{2+}-activated K^+ channel (maxi-K^+) found in *Drosophila slowpoke. B*, expression of exogenous hTTYH3 protein by Western blot. *Upper panel*, the protein (20 μg) in each lane was separated by conventional SDS-PAGE. The immune complexes with the antibody (1:1000) were detected by horseradish peroxidase-labeled anti-rabbit IgG (1:10,000) by using an ECL detection system. The *upper arrow* indicates the glycosylation form of hTTYH3, and the *lower arrow* indicates the predicted 58 kDa of hTTYH3. *Left panel*, lane CHO, control CHO; *hTTY3*, hTTYH3-transfected CHO; + *glycanase*, digestion with *N*-glycanase of hTTYH3-transfected CHO; *number-T/A*, mutant possessing Ala substituted with Thr at the position of the number was transfected into CHO. *Right panel*, *lane HEK*, control HEK; *hTTY3*, hTTYH3-transfected HEK. *Lower panel*, the panel on the *left* shows the same membrane as above. The membrane was washed in SDS containing boiled DW and re-probed with the same antibody with an excess amount of antigen. *C*, histologic staining was performed and detected by FITC-labeled anti-rabbit IgG. The image of the cells was viewed with fluorescence microscopy (*left panels*) or with Nomarski optics (*right panels*). CHO cells were transfected by hTTYH3 (*upper panels*). Endogenous hTTYH3 was detected in HEK cells (*middle panels*). The immunoreactivity remarkably decreased in HEK cells incubated with an excess amount of antigen (*Ag*) (*lower panels*).

Localization of hTTYH and mTTYH3—hTTYH3 and mTTYH3 are distributed mainly in excitable tissues. hTTYH3 mRNA of 4.8 kb was found by Northern blotting in the brain, heart, skeletal muscle, colon, spleen, kidney, and peripheral blood leukocytes (Fig. 2*A*). RT-PCR using mouse tissues revealed positive signals also in fat, the pancreas, thymus, and uterus (Fig. 2*B*). mTTYH3 was also detected in an endothelial cell line, kidney epithelial cells (opossum kidney and HEK), and a neuronal cell line (PC12 and N2A). To confirm the absence of a hamster *c*TTYH3 product in CHO cells, we cloned a partial sequence of hamster *c*TTYH3 (AB158504), 84 amino acids, from genomic DNA of CHO cells by PCR (*arrows* in Fig. 1*A*). A comparison of the hamster sequence with those of other species showed that one and nine amino acids differed from those in mouse and human, respectively. By using species-common primers, *c*TTYH3 cDNA was not found in CHO by RT-PCR.

Immunohistological analysis was performed on mouse tissues (Fig. 3). Thalamic neurons and ventricular cells of the heart and skeletal muscle membrane were positively stained. A negative control was obtained with an excess of antigen. In the kidney, cells in glomeruli, presumably mesangium cells, were positively stained. Although opossum kidney cells or HEK cells showed positive hmcTTYH3 signals by RT-PCR, renal proximal tubules were not positively stained. The signal may be indis-

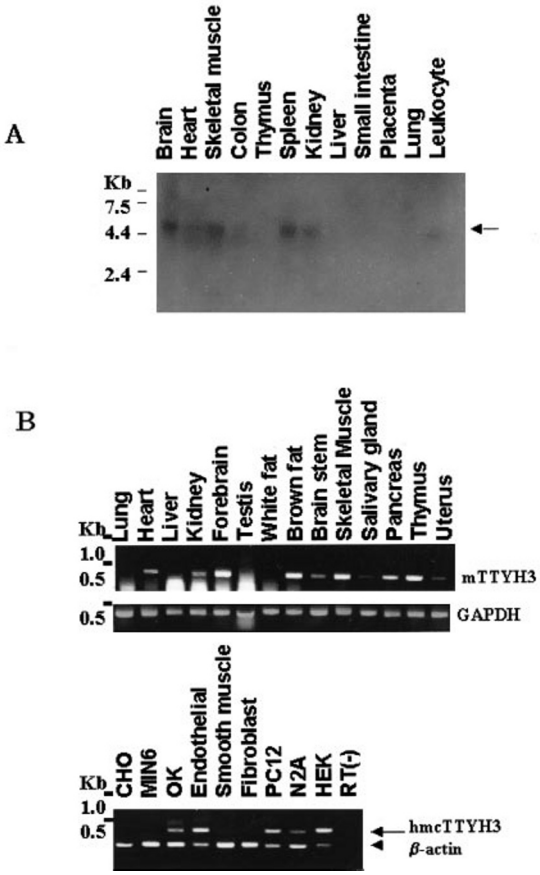

FIG. 2. **Localization of hTTYH3 and mTTYH3.** *A*, results of Northern blot analysis of hTTYH3 in human tissues are shown. The membrane was incubated with a ^{32}P-labeled hTTYH3 fragment. The *arrow* indicates hTTYH mRNA of 4.8 kb. *B*, RT-PCR analysis of denoted mouse tissues and cell line. The primer sets were designed commonly to detect human, mouse, and hamster hmcTTYH3 fragments. RT-PCR was performed bye conventional method. Mouse glyceraldehyde-3-phosphate dehydrogenase (*GAPDH*) was used for the control amplification of tissue cDNA in the *upper panel*, and β-actin cDNA was used for the control of the cell lines in the *lower panel*. *RT*(−) indicates the result obtained by the same procedure using HEK as a template without reverse transcriptase.

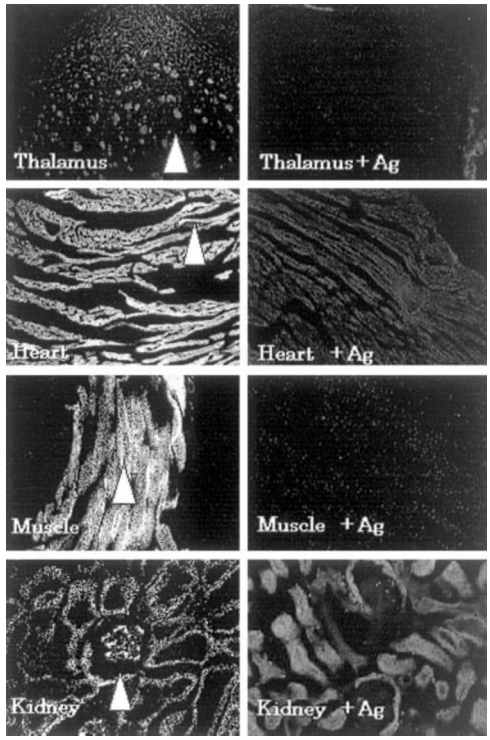

FIG. 3. **Immunohistochemical staining of representative tissues.** Immunoreactivity was detected in tissues. The primary C-terminal antibody was diluted 1:100 and detected with FITC-labeled anti-rabbit antibody (1:1000). Thalamic portions of the brain, heart, renal cortex, and skeletal muscle are shown. Negative controls with an excess of antigen (*Ag*) are shown on the *right*. They were viewed through a microscope (×200), and the photos were converted into white and black images (Photoshop version 7, Macintosh). Positive signals are indicated by *triangles*.

tinguishable because the level of autofluorescence of proximal tubules is high and/or the level of expression of mTTYH3 is low in this segment. Therefore, mTTYH3 is located mainly in excitable membranes.

Whole Cell Recordings of hTTYH3-transfected CHO Cells—We first selected HEK293 cells for the expression of hTTYH3, because HEK293 cells were used for discovery of the ClCA family (10). When transiently expressed in HEK293 cells, hTTYH3 was associated with a prominent Cl^- current that was activated by ionomycin (10^{-6} M). The current was much less marked in GFP vector (mock)-transfected cells. However, a similar large conductance Cl^- single channel (12) was detected in the following investigation. Therefore, we used CHO cells.

The basal current in hTTYH3-transfected CHO cells was not different from that in untransfected control cells. Although ionomycin induced an outward-rectified current in mock-transfected cells, it induced an overt linear current in hTTYH3-transfected cells (Fig. 4*A*). The current was not altered by substitution of sodium with TEA but was altered by substitution of Cl^- with gluconate in the bath solution, suggesting that the current is a current driven by an anion. The permeability ratio of Cs^+/Cl^- was nominally zero and that of gluconate/Cl^- was 0.33 (15).

To investigate the ion selectivity, we used whole cell patches with a pipette solution containing 0.5 mM $CaCl_2$, because this large amount of Ca^{2+} was required to stabilize the current-voltage relation. The ionic selectivity was altered in hTTYH3 pore mutants by exchanges of charged amino acids (Fig. 4*B*). Mutant H370D showed a different selectivity, in which gluconate/Cl^- decreased from 0.3 to 0.12 and Cs^+/Cl^- increased to 0.1. Mutant R366Q was more permeable to cations. The reversal potential with isosmotic NaCl/CsCl shifted to 12.5 mV (mean of eight), suggesting significant permeability to Na^+. Assuming that TEA and gluconate are impermeable ions, the $Na^+/Cs^+/Cl^-$ permeability ratio was calculated to be 0.7:0.25:1. Thus, positively charged amino acids at positions 366 and 370 composed the pore of hTTYH3, playing a role in anion selectivity.

Halide selectivity of hTTYH3 was precisely measured by single channel analysis. Anions in the pipette solution were changed in each experiment, and reversal potential was measured ($n = 5$ in each). The resultant order of permeability (P_X/P_{Cl^-}) was I^- (2.2), Br^- (1.8), SCN^- (1), NO_3^- (0.83), gluconate$^-$ (0.3), aspartate$^-$ (0.2), and Na^+ (<0.1).

Effects of Blockers on the hTTYH3 Channel—The effects of blockers were investigated next. The evoked current in non-transfected cells was blocked by niflumate, whereas the evoked current in hTTYH3-transfected cells was not inhibited by niflumate (300 μg/ml). The CaC current was not inhibited by 10 μM dithiothreitol, 10 μM $ZnCl_2$, or 10 μM SITS but was completely inhibited by 10 μM DIDS (Fig. 4*C*, *left*). Effects of reagents on the single hTTYH3 channel in an inside-out configuration were also examined. Niflumate had no effect ($P_o = 0.8$ to 0.82, $n = 4$). SITS induced a flickering opening but had no significant inhibitory effect ($P_o = 0.58$, $n = 4$), whereas DIDS induced a blockade ($P_o = 0.12$, $n = 0.4$, $p < 0.01$) within a few

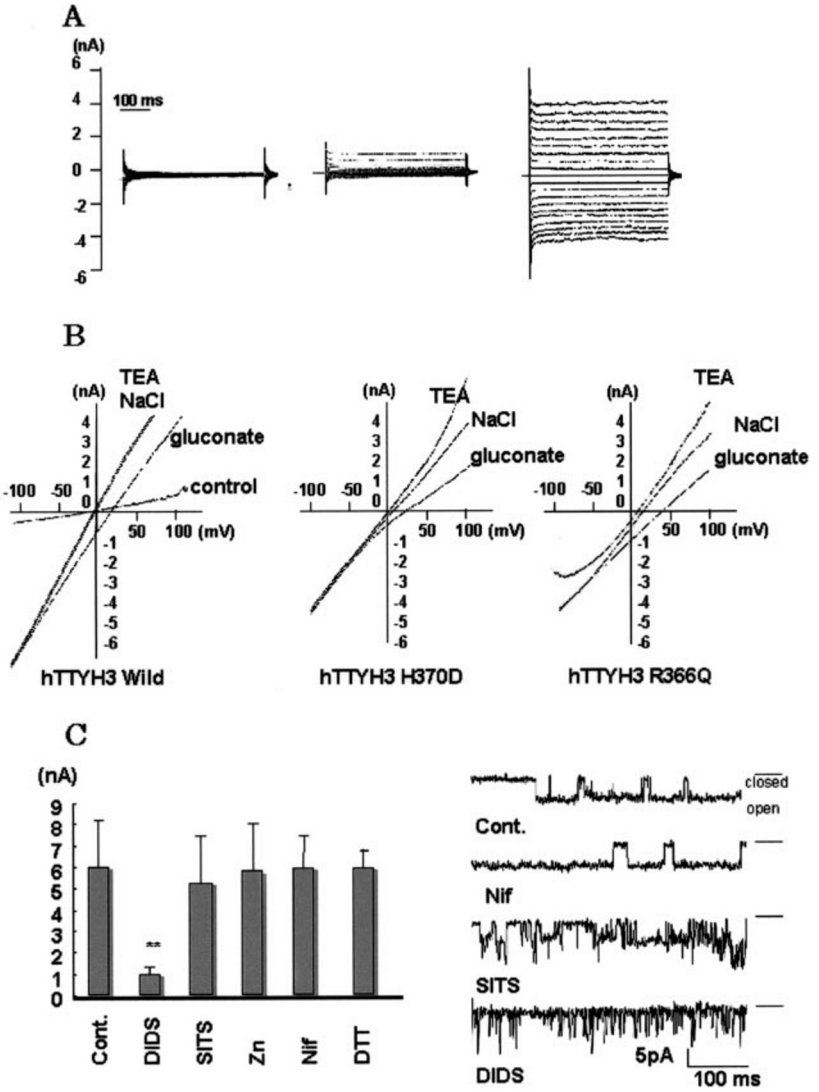

FIG. 4. **Whole cellular current of hTTYH3 in CHO cells and effects of blocking reagents.** *A*, currents were recorded from −100 to +90 mV at steps of 10 mV in control CHO cells (*left*) and cells treated with ionomycin (*center*). The hTTYH3-transfected cells were treated with ionomycin (*right*). *B*, the current-voltage relation was obtained by ramp pulses from −120 to 120 mV. *Left*, representative current-voltage relation of control cells and wild hTTYH3-transfected cells treated with ionomycin (NaCl). Then the bath solution was changed to TEACl (*TEA*) or sodium gluconate (*Gluconate*). The current-voltage relation was obtained from H370D (*center*) or from R366Q (*right*) mutant-transfected cells. *C*, *left*, effects of blocking reagents on the hTTYH3 current are shown as the magnitude of the current at +100 mV ($n = 8$). **, $p < 0.01$. *Right*, effects of blocking reagents on an hTTYH3 single channel. Single channel traces at −30 mV were recorded in an inside-out configuration. Blockers were added to the cytosolic side. *Cont.*, control hTTYH3-transfected cells; *Nif*, niflumic acid; *Zn*, $ZnCl_2$; *solid* and *dashed lines*, opened and closed states, respectively.

seconds (Fig. 4*C, right*). Therefore, the hTTYH3 current was only sensitive to DIDS.

Single Channel Analysis of hTTYH3—hTTYH3 was characterized by single channel analysis. Maxi-Cl^- channel activity was observed within 30 s after detachment of the membrane when bath solution contained 0.1 mM of Ca^{2+} (Fig. 5*A*). Such a large conductance was observed in hTTYH3-transfected cells but not in non-transfected cells. The current-voltage relation was linear in symmetrical Cl^- solution ($n = 12$) with slope conductance of 260 pS (Fig. 5*B*). Open probability was not dependent on voltage of less than 0 mV but decreased at voltage over 60 mV (Fig. 5*C*). The distribution of current amplitudes fitted well to results of Gausian's analysis, indicating a subconductance of 50 pS (Fig. 5*D*). The channel had a long open lifetime as was observed in the trace at +40 mV, whereas it also had a fluctuating rapid opening as was observed in the trace at −60 mV. Long opening and rapid (but transient) fluctuations were observed in the same patch membrane. The hTTYH3 channel therefore involved a multiopening mechanism. Open-closed lifetimes fit better to two kinetic states ($\tau o1 = 52$, $\tau o\ 2 = 510$ ms, $\tau c1 = 60$ and $\tau c2 = 250$ ms, mean of 12) rather than 1.

As in the case of a maxi-K^+ channel (17) and ClCA channel (10), a high concentration of cytosolic Ca^{2+} was essential for hTTYH3 activation. The open probability was plotted against Ca^{2+} concentration, resulting in an ED_{50} of about 2 μM (Fig. 5*E*). The range of Ca^{2+} concentrations is similar to that for maxi-K^+ activation (18). The value 2 μM is within the physiologic range of Ca^{2+} in excitable cells in which hTTYH3 is detected. Thus, like the maxi-K^+ channel, hTTYH3 may play a role in Ca^{2+} signal transduction.

However, it took around 10 s for activation when the cytosolic side of the isolated membrane was exposed to high Ca^{2+} solution. Thus, protein phosphorylation or another complex mechanism might be involved in the activation. To search for activators, activity of hTTYH3 was observed in a cell-attached configuration with stably transformed CHO cells, and the presence of hTTYH3 channels in the attached membrane was determined later in an inside-out configuration in high Ca^{2+} solution. Although protein kinase sites on the amino acid sequences were predicted, direct opening of the hTTYH3 channel by protein kinase A (dibutyryl cAMP, 10^{-5} M) or kinase C (phorbol ester, 10^{-8} M) was not observed. Addition of staurosporine (10^{-6} M), GTPγS (10^{-5} M), or okadaic acid (10^{-5} M) to the bath solution did not activate the hTTYH3 channel (data not shown). Therefore, the physiological role of hTTYH3 remains obscure and awaits *in vivo* study.

Expression and Activation of hTTYH1 and hTTYH2 Channels—To elucidate the physiological role of the TTYH family, we examined the functional expression of other members, hTTYH1 and hTTYH2. Based on the above results, we tested whether hTTYH1 and hTTYH2 were also expressed as evoked

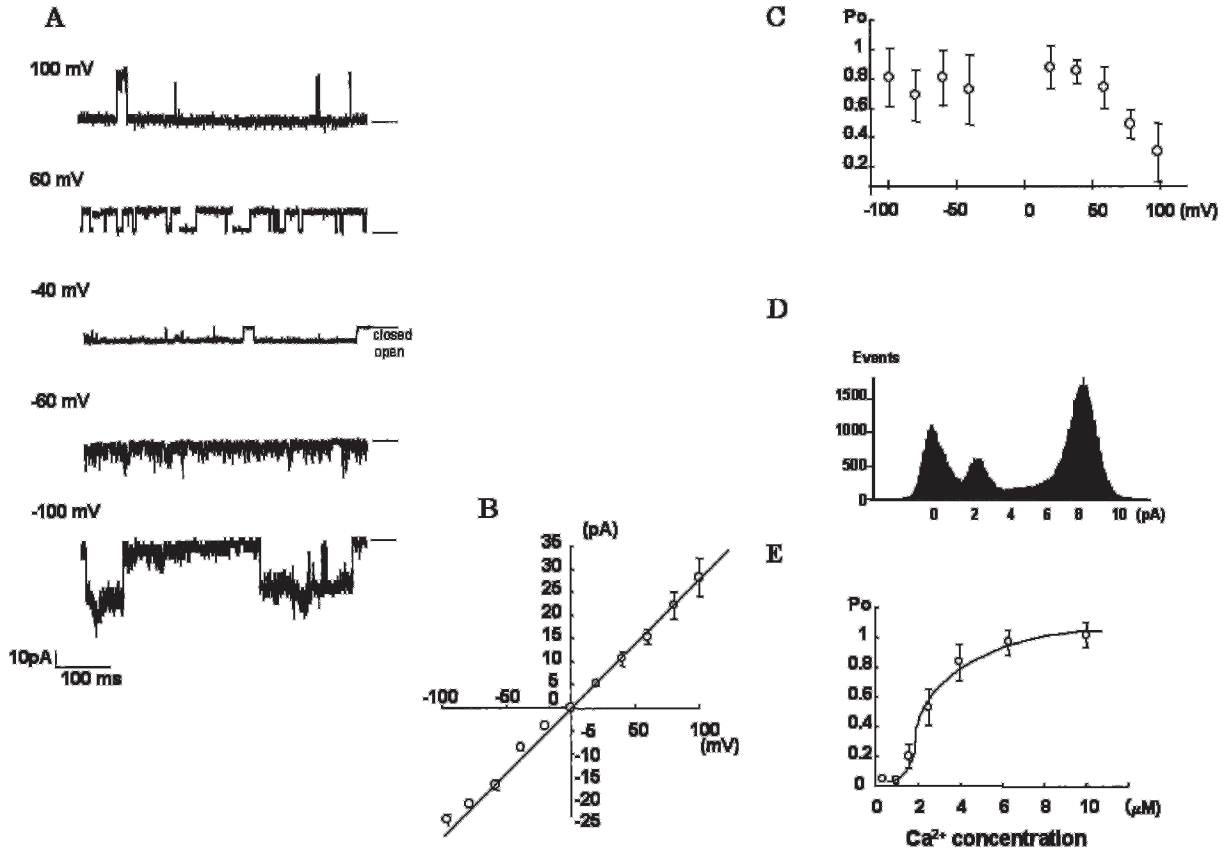

FIG. 5. **Single hTTYH3 channel.** *A*, representative single channel traces at the given voltage in the same patch membrane are shown. *Solid* and *dashed lines* indicate opened and closed states, respectively. *B*, mean ± S.E. of magnitude of the current is plotted against membrane voltage (n = 12). *C*, open probability is plotted against membrane voltage. *D*, the frequency of observation (events) is plotted against the magnitude of current accumulated over a period of 30 s at a voltage of 40 mV. *E*, open probability in hyperpolarized voltage at −80 mV was measured at various cytosolic calcium concentrations (mean ± S.E., n = 6).

Cl^- channels (Fig. 6). Activity of the hTTYH1 single channel was sometimes observed in cell-attached patches, showing slope conductance of 280 pS. However, the hTTYH2-induced channel appeared only after treatment with ionomycin. hTTYH2 was expressed as a Ca^{2+}-dependent inward-rectified Cl^- channel of 120 pS in an inward direction and of 45 pS in an outward direction. In a cell-attached configuration, reversal potential of hTTYH1 and hTTYH2 was around −30 mV, which is similar to the Cl^- equilibrium potential. By substitution of NaCl with TEA-Cl in a pipette solution, the permeability ratio, P_{Na}/P_{Cl}, was calculated to be less than 0.1 for hTTYH1 and 0.1 for hTTYH2.

We next tested the influence of a hypotonic solution on hTTYH1 and hTTYH3 channels. In a whole cell configuration with CsCl in the pipette solution without Ca^{2+} (pCa = 7.2), the current by hTTYH1 was usually silent but remarkably activated when the bath osmolarity was changed to a hypotonic solution of 250 mOsm (Fig. 7*A*). The current was further activated in a hypotonic solution of 220 mOsm. A whole cellular current-voltage relation of hTTYH1 in a hypotonic solution was not obtained because the magnitude of the current was unstably high. Because the current at 0 mV was stable even in a hypotonic solution, this prominent current was not due to leakage but due to fluctuated opening and closing of the large channel. The current magnitude at 100 mV was measured (n = 6, Fig. 7*B*). The evoked current at 220 mOsm was diminished by 50 μM $GdCl_3$ and abolished by 10 μM DIDS. On the other hand, the current of hTTYH3-expressed cells was significantly activated only when exposed to a solution of 220 mOsm. The evoked current was blocked by 50 μM $GdCl_3$. This magnitude of activation in a hypotonic solution was, however, observed in GFP-transfected control CHO cells (19). Thus, we conclude that hTTYH1 is involved in a swelling-activated Cl^- channel, whereas hTTYH3 may not be involved. Thus, the common feature of these three channels is large conductance.

DISCUSSION

In this study, we showed that the hTTYH family possesses 5 or 6 transmembrane segments encoding a large conductance Cl^- channel. The structure of hTTYH3 was estimated by computer-based hydrophobic analysis, addition of tag alignment, and glycosylation scanning. The results of a mutation study suggested that the structure of this novel maxi-Cl^- channel is similar to the structure of known cation channels, in which a selective pore is located between TMS5 and TMS6 and a regulatory domain is located in the C terminus. An ion channel with the pore domain between TMS5 and TMS6 is a prototype structure of cation-permeable channels, such as the K^+ channel encoded by the Kv family and the Ca^{2+} channel encoded by the Trp family (20). These molecules have been discovered from abnormal behavior of the fruit fly, *Drosophila*. The hTTYH family may also become a prototype of the Cl^- channel, because hTTYH1–3 showed comparable structure and function.

Discrimination between endogenous and exogenous CaC currents was usually difficult. Fortunately, hTTYH3 encoded a characteristic large conductance channel, which was not observed in CHO cells. The magnitude of the endogenous current evoked by ionomycin does not exceed 1 nA at 100 mV in CHO cells (21, 22), compared with that shown around 4 nA in hTYY3-transfected CHO cells. hTTYH1 and hTTYH2 induced

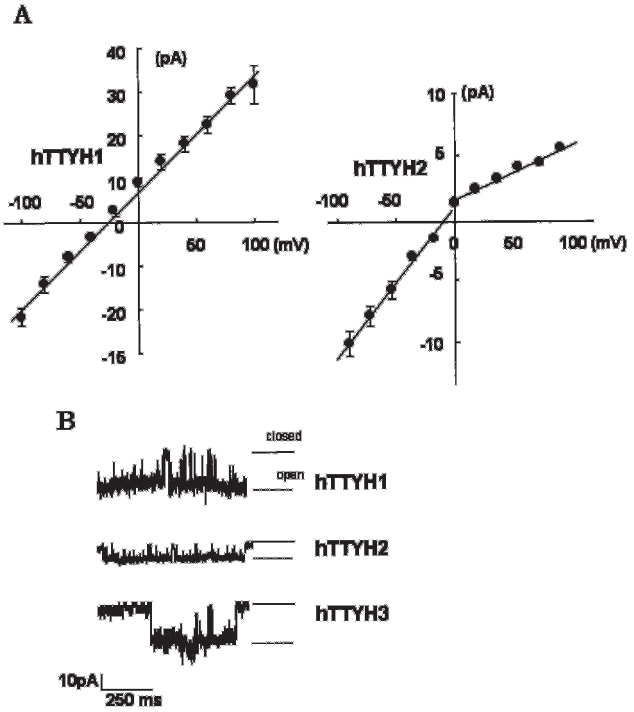

FIG. 6. **Single hTTYH1 and hTTYH2 channels.** *A*, hTTYH1 and hTTYH2 channels were recorded in a cell-attached configuration. Single channel of hTTYH2 was observed after addition of ionomycin (10^{-6} M) to the bath, whereas hTTYH1 was sometimes observed without any manipulation. Mean ± S.E. of magnitude of the single channel current is plotted against membrane voltage ($n = 4$). *B*, representative traces of hTTYH1, -2, and -3 (the same as in Fig. 5) at −100 mV in a cell-attached configuration are shown. *Solid* and *dashed lines* indicate opened and closed states, respectively.

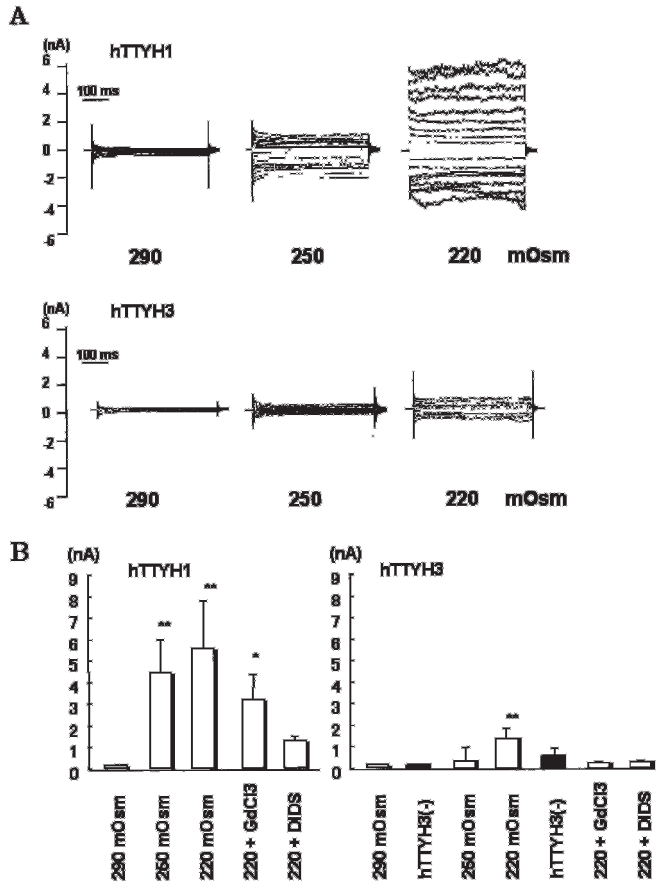

FIG. 7. **Effects of hypotonic media on hTTYH1 and hTTYH3 currents.** *A*, whole cellular currents were recorded with CsCl and without $CaCl_2$ in pipette solution from −100 to +90 mV at steps of 10 mV in hTTYH1-transfected (*upper panel*) and hTTYH3-transfected (*lower panel*) CHO cells. The bath solution was changed to hypotonic solutions of 250 and 220 mOsm. *B*, magnitude of the current at 100 mV was measured in six experiments with hTTYH1 current (*left panel*) and with hTTYH3 current (*right panel*). Significant increase compared with the control (290 mOsm) is indicated by an *asterisk* (analysis of variance, *, < 0.05; **, <0.001). *220 + GdCl$_3$* and *220 + DIDS* indicate that 50 μM of $GdCl_3$ and 10 μM of DIDS were dissolved in 220 mOsm solution, respectively. *TTYH3*(−) indicates the endogenous current of CHO cells exposed to solutions of 290 and 220 mOsm.

currents that were different in conductance and in dependence of Ca^{2+}. hTTYH1 encoded a Ca^{2+}-independent large current around 5 nA that was induced by a hypotonic solution. This swelling-activated current was neither observed endogenously (19) nor in hTYYH3-transfected CHO cells. Furthermore, the results of the study using mutants strongly suggested that the large conductance was induced by exogenous, not endogenous, hTTYH3 cDNA because exogenous mutants altered the whole cell current. Therefore, hTTYH-induced currents observed in this study were endowed exogenously by cDNA.

The channel encoded by hTTYH3 showed characteristics similar to those of maxi-Cl^- channels *in situ*. First, most Cl^- channels are blocked by niflumic acid at a concentration of 300 μg/ml (3). Activity of maxi-Cl^- is, however, blocked by DIDS or SITS (4, 5, 23). Second, voltage-dependent suppression at high depolarization is observed in hTTYH3 and in some CaC channels (1, 24, 25). However, the voltage-dependent suppression of the maxi-Cl^- channel is characterized as a "bell-shaped" relation; suppression to the opening is observed in highly depolarized and in deep repolarized potentials (26). The current-voltage relation of the hTTYH3 channel did not show bell-shaped suppression because suppression at deep negative potential was not observed. Furthermore, it is still not clear why open probability of the channel was decreased despite the fact that the whole cellular current was not decreased at a highly depolarized potential. The depolarization might increase the number of open channels but decrease the probability of opening. A subunit might be needed to solve the discrepancy in voltage dependence. Third, maxi-Cl^- channels have complex mechanisms of conductance (1, 27) and lifetime kinetics (25, 28). Fourth, the hTTYH3 channel displayed a permeability sequence of $I^- > Br^- > Cl^-$, which was observed in skeletal muscle (29) and corresponds to Eisenman's sequence. The ionic environment within the channel is, however, influenced by the cationic environment, which alters the selective order of Cl^- channels (26), suggesting that this order of permeability may not be specific for the hTTYH3 structure.

hTTYH3 may encode a Ca^{2+}-activated maxi-Cl^- channel in the excitable membrane. A maxi-Cl^- channel in worm, amphibian, or rat lactotrophs was found to be activated directly by cytosolic Ca^{2+} (2, 25, 28). However, there is argument against a direct ligand-type Ca^{2+} dependence in the activation of maxi-Cl^- channels. Some maxi-Cl^- channels are activated by polymyxin B, an inhibitor of protein kinase C (6), G-protein (24), or okadaic acid (30). Although we used various reagents to investigate the regulation, none of them activated the hTTYH3 channel. Further studies are required to clarify the regulation.

hTTYH3 cDNA as well as protein was found in HEK293 cells. However, Ca^{2+}-dependent maxi-Cl^- channels in HEK cells were not discovered previously. The Ca^{2+}-independent maxi-Cl^- channel of HEK cells (12) exhibits an outward-rectified property. It is similar in conductance but not similar in characteristics to the hTTYH3 channel. Results of Western blot analysis suggested that the amount of endogenous hTTYH3 protein was small, and this might have been the reason why an

hTTYH3-like channel was not discovered in previous electrophysiologic studies. An hTTYH3-like channel may not be expressed in the plasma membrane of HEK cells *in situ*.

On the other hand, hTTYH1-like Ca^{2+}-independent large conductance Cl^- channels have been frequently observed in mammalian cells such as HEK293 cells (12), smooth muscle (23, 31), T-lymphocytes (32), endothelial cells (3), and cardiac myocytes (27). The maxi-Cl^- channels in the latter two are activated in hypotonic media. The physiological role of a swelling-activated anion channel has been described in detail (8). A hypotonic solution induces gain of cell volume, which is restored by K^+ and Cl^- exit from the cell interior in concert. Volume-sensitive (swelling-activated) Cl^- channels play a cardinal role in this phenomenon. A direct contribution of volume-sensitive Cl^- channels to the physiological situation has also been described. Recently, Bell *et al.* (33) suggested that a volume-sensitive maxi-Cl^- channel in macula densa cells plays an important role in tubulo-glomerular feedback. This finding provides a new insight into the physiological role of the volume-sensitive maxi-Cl^- channel as a regulator of body fluid homeostasis. hTTYH1 may be involved in this class of channels, because activation by hypotonic media was observed in the physiological range or at least in the same range as that used in previous experiments (27, 34). We sometimes observed single channel activity of hTTYH1 in cell-attached patches, probably because the cell volume was changed during patch-clamping manipulation. Therefore, it would be interesting to clarify the localization of hTTYH1 molecules, mechanism of regulation, availability of ATP carriers, and molecular mechanism of osmosensing. Such studies should be performed in the future. Based on the functional expression of hTTYH1 and hTTYH3, the tweety family encodes a large conductance Cl^- channel that is similar to the maxi-Cl^- channel found in various cells.

The activation of hTTYH2 and hTTYH3 channels requires a high concentration of Ca^{2+}, whereas hTTYH1 encodes a Ca^{2+}-independent volume-sensitive Cl^- channel. In our computer-based homology search, only three members (hTTYH1–3) were found. A homology tree among these three channels revealed that hTTYH3 is more homologous to hTTYH2 than to hTTYH1. The C-terminal region of hTTYH1 is shorter than those of the other two. Based on these comparisons, hTTYH3 is structurally and functionally more similar to hTTYH2 than to hTTYH1. Thus, more members similar to hTTYH1 may be discovered in the future. Investigation of this family will reveal the molecular mechanism and the physiologic role of the large conductance Cl^- channel family irrespective of calcium dependence.

Acknowledgments—We thank Y. Oyama and M. Hashimoto for their excellent technical assistance and editorial work.

Note Added in Proof—Sequences of isolated clones used in the expression study have been deposited in GenBank™ (hTTYH3, AB162931; hTTYH2, BC005168; hTTYH1s, AB162929; and mTTY1s, AB162930). The hTTYH1s, encoding the volume-sensitive Cl channel, is a C-terminal spliced variant of ttyh1 (NM020659). Exon 11 is skipped in hTTYH1s. Expression of hTTYH1 did not show the volume-sensitive Cl^- current.

REFERENCES

1. Thorn, P., and Martin, R. J. (1987) *Q. J. Exp. Physiol.* **72,** 31–49
2. Fahmi, M., Garcia, L., Taupignon, A., Dufy, B., and Sartor, P. (1995) *Am. J. Physiol.* **269,** E969–E976
3. Nilius, B., and Droogmans, G. (2001) *Physiol. Rev.* **81,** 1415–1549
4. Kemp, P. J., MacGregor, G. G., and Olver, R. E. (1993) *Am. J. Physiol.* **265,** L323–L329
5. Sun, X. P., Supplisson, S., Torres, R., Sachs, G., and Mayer, E. (1992) *J. Physiol.* (*Lond.*) **448,** 355–382
6. Groschner, K., and Kukovetz, W. R. (1992) *Pfluegers Arch.* **421,** 209–217
7. Schwiebert, E. M., Benos, D. J., Egan, M. E., Stutts, M. J., and Guggino, W. B. (1999) *Physiol. Rev.* **79,** S145–S166
8. Jentsch, T. J., Stein, V., Weuinreich, F., and Zdebik, A. A. (2002) *Physiol. Rev.* **82,** 503–568
9. Yasui, M., Hazama, A., Kwon, T. H., Nielsen, S., Guggino, W. B., and Agre, P. (1999) *Nature* **402,** 184–187
10. Gandhi, R., Elble, R. C., Gruber, A. D., Ji, H. L., Copeland, S. M., Fuller, C. M., and Pauli, B. U. (1998) *J. Biol. Chem.* **273,** 32096–32101
11. Gruber, A. D., Elble, R. C., Ji, H. L., Schreur, K. D., Fuller, C. M., and Pauli, B. U. (1998) *Genomics* **54,** 200–214
12. Zhu, G., Zhang, Y., Xu, H., and Jiang, C. (1998) *J. Neurosci. Methods* **81,** 73–83
13. Maleszka, R., Hanes, S. D., Hackett, R. L., DeCouet, H. G., and Gabormiklos, G. L. (1996) *Proc. Natl. Acad. Sci. U. S. A.* **93,** 447–451
14. Suzuki, M., Morita, T., Hanaoka, K., Kawaguchi, Y., and Sakai, O. (1991) *J. Clin. Investig.* **83,** 735–742
15. Hille, B. (1992) *Ionic Channels of Excitable Membranes,* 2nd Ed., pp. 337–361, Sinauer Associates, Inc., Sunderland, MA
16. Campbell, H. D., Kamei, M., Claudianos, C., Woollatt, E., Sutherland, G. R., Suzuki, Y., Hida, M., Sugano, S., and Young, I. G. (2000) *Genomics* **68,** 89–92
17. Piskorowski, R., and Aldrich, R. W. (2002) *Nature* **420,** 500–503
18. Schreiber, M., Yuan, A., and Salkoff, L. (1999) *Nat. Neurosci.* **2,** 416–421
19. Suzuki, M., Mizuno, A., Kodaira, K., and Imai, M. (2003) *J. Biol. Chem.* **278,** 22664–22668
20. Minke, B., and Cook, B. (2002) *Physiol. Rev.* **82,** 429–472
21. Zitt, C., Obukhov, A. G., Strübing, C., Zobel, A., Kalkbrenner, F., Lückhoff, A., and Schultz, G. (1997) *J. Cell Biol.* **138,** 1333–1341
22. Zhou, X. B., Ruth, P., Schlossmann, J., Hofmann, F., and Korth, M. (1996) *J. Biol. Chem.* **271,** 19760–19767
23. Kokubun, S., Saigusa, A., and Tamura, T. (1991) *Pfluegers Arch.* **418,** 204–213
24. Sun, X. P., Supplisson, S., and Mayer, E. (1993) *Am. J. Physiol.* **264,** G774–G785
25. Hussy, N. (1992) *J. Neurophysiol.* **68,** 2024–2050
26. Hurnak, O., and Zachar, J. (1993) *Gen. Physiol. Biophys.* **12,** 171–182
27. Coulombe, A., and Coraboeuf, E. (1992) *Pfluegers Arch.* **422,** 143–150
28. Dixon, D. M., Valkanov, M., and Martin, R. J. (1993) *J. Membr. Biol.* **131,** 143–149
29. Wright, E. M., and Diamond, J. M. (1977) *Physiol. Rev.* **57,** 109–156
30. Diaz, M., Bahamonde, M. I., Lock, H., Munoz, F. J., Hardy, S. P., Posas, F., and Valverde, M. A. (2001) *J. Physiol.* (*Lond.*) **536,** 79–88
31. Pacaud, P., Loirand, G., Gregoire, G., Mironneau, C., and Mironneau, J. (1992) *Pfluegers Arch.* **421,** 125–130
32. Pahapill, P. A., and Schlichter, L. C. (1992) *J. Membr. Biol.* **125,** 171–183
33. Bell, P. D., Lapointe, J. Y., Sabirov, R., Hayashi, S., Peti-Peterdi, J., Manabe, K., Kovacs, G., and Okada, Y. (2003) *Proc. Natl. Acad. Sci. U. S. A.* **100,** 4322–4327
34. Sabirov, R. Z., Dutta, A. K., and Okada, Y. (2001) *J. Gen. Physiol.* **118,** 251–266